



# Significant seismic anisotropy beneath the southern Lhasa Terrane, Tibetan Plateau

Stephen S. Gao and Kelly H. Liu

*Department of Geological Sciences and Engineering, Missouri University of Science and Technology, Rolla, Missouri 65409, USA (sgao@mst.edu; liukh@mst.edu)*

[1] Shear wave splitting measurements using teleseismic PKS, SKKS, and SKS phases recorded by station LSA on the southern part of the Lhasa Terrane of the Tibetan Plateau reveal significant azimuthal anisotropy with a splitting time of up to 1.5 s, a conclusion that is contradictory to previous studies which suggested isotropy or weak anisotropy. In addition, systematic variations of the splitting parameters (fast polarization direction and splitting time) with the arriving azimuth of the seismic ray path are observed, suggesting a model of anisotropy that is more complicated than a single layer with horizontal axis of symmetry. The measurements are consistent with a model with two layers of anisotropy. The top layer has a NE-SW fast direction, which is consistent with GPS-revealed direction of surface movement, and can be associated with lattice preferred orientation of middle-lower crustal minerals such as amphibole. The lower layer has a nearly E-W fast direction and can be the consequence of either the N-S directed compressional stress originated from the India-Eurasia collision or flow in the asthenosphere related to the absolute motion of Eurasia. This study underlines the importance of a long duration of deployment of seismic stations in resolving complex anisotropy.

**Components:** 7125 words, 12 figures, 1 table.

**Keywords:** seismic anisotropy; Tibetan Plateau; mantle flow; amphibole; GPS.

**Index Terms:** 7218 Seismology: Lithosphere (1236); 7205 Seismology: Continental crust (1219); 7208 Seismology: Mantle (1212, 1213, 8124).

**Received** 2 September 2008; **Revised** 10 November 2008; **Accepted** 31 December 2008; **Published** 12 February 2009.

Gao, S. S., and K. H. Liu (2009), Significant seismic anisotropy beneath the southern Lhasa Terrane, Tibetan Plateau, *Geochem. Geophys. Geosyst.*, 10, Q02008, doi:10.1029/2008GC002227.

## 1. Introduction

[2] The Lhasa Terrane of the Tibetan Plateau (Figures 1 and 2) is located between the Bangong-Nujiang suture (BNS) in the north and Indus-Yalu suture (IYS) in the south, which separates rocks of Indian and Asian origin [Yin and Harrison, 2000]. Over the past 30 years many geophysical experiments have been conducted in the area. Receiver function studies found that the area has a crustal

thickness of 85 km, which is among the thickest on Earth [Owens and Zandt, 1997]. A partially molten middle crust, approximately in the depth range of 10 to 30 km, is revealed by inversion of teleseismic receiver functions [Kind *et al.*, 1996]. Gravity isostasy studies suggest that the thickness of the lithosphere beneath the Lhasa Terrane is up to 260 km, which is significantly thicker than that beneath the Qiangtang Terrane north of the BNS, and nearly doubles that of the Indian plate [Jimenez-Munt *et al.*, 2008]. Most seismic tomography

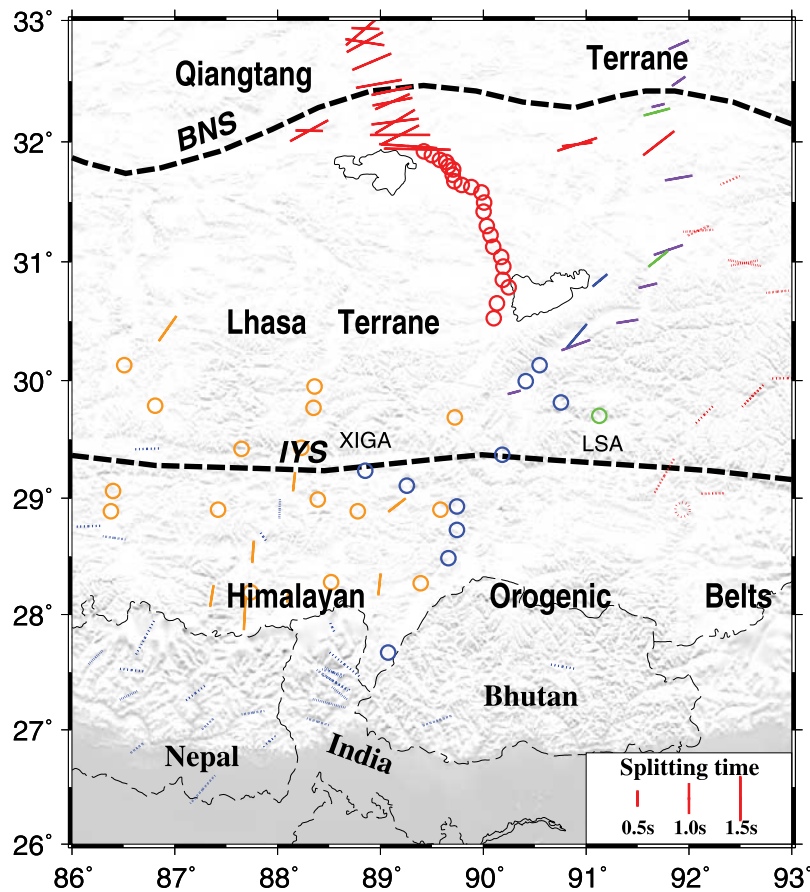


**Figure 1.** Map showing the major tectonic provinces and previous shear wave splitting measurements in the Lhasa Terrane and adjacent areas. The orientation of the bar represents the fast polarization direction, and the length of the bar is proportional to the splitting time. Circles are null measurements. Red solid symbols, *Huang et al.* [2000]; red dashed symbols, *Sol et al.* [2007]; green, *McNamara et al.* [1994]; blue solid symbols, *Sandvol et al.* [1997]; blue dashed symbols, *Singh et al.* [2007]; purple, *Hirn et al.* [1995]; and orange, *Fu et al.* [2008].

studies also revealed the existence of the subducted Indian lithosphere beneath southern Lhasa Terrane [*Li et al.*, 2006; *Tilmann et al.*, 2003].

[3] Splitting of P-to-S converted phases at the core-mantle boundary such as PKS, SKKS, and SKS (hereafter collectively referred to as XKS) is increasingly used to infer the lattice preferred orientation (LPO) of anisotropic minerals in the Earth's crust and mantle [*Silver*, 1996; *Savage*, 1999; *Fouch and Rondenay*, 2006]. In the upper mantle, A-type LPO of olivine is believed to be the major cause of observed seismic anisotropy. The polarization direction of the fast wave (i.e., the fast direction  $\phi$ ) is parallel to the flow direction or is orthogonal to the direction of maximum compression [*Zhang and Karato*, 1995; *Mainprice et al.*, 2000]. LPO can also form for crustal minerals such as amphibole under plastic flow, with a fast direction being parallel to the flow direction [*Tatham et al.*, 2008; *Aspiroz et al.*, 2007]. While most moun-

tain belts on Earth possess significant seismic anisotropy with a dominantly strike-parallel fast direction [*Silver*, 1996], virtually all the previous studies concluded that the mantle beneath the southern Lhasa Terrane, which has been under considerable N-S oriented compressional strain over the past tens of millions of years, is surprisingly isotropic or weakly anisotropic. This study is aimed at resolving this puzzling controversy.

## 2. Previous Shear Wave Splitting Measurements on the Tibetan Plateau and Adjacent Areas

[4] Numerous shear wave splitting studies have been performed on the Tibetan Plateau and adjacent areas (Figure 1). The first shear wave splitting analysis on the Indian continent was conducted by *Vinnik et al.* [1992], who reported a nearly E-W fast direction and a significant splitting time of 1.1 s

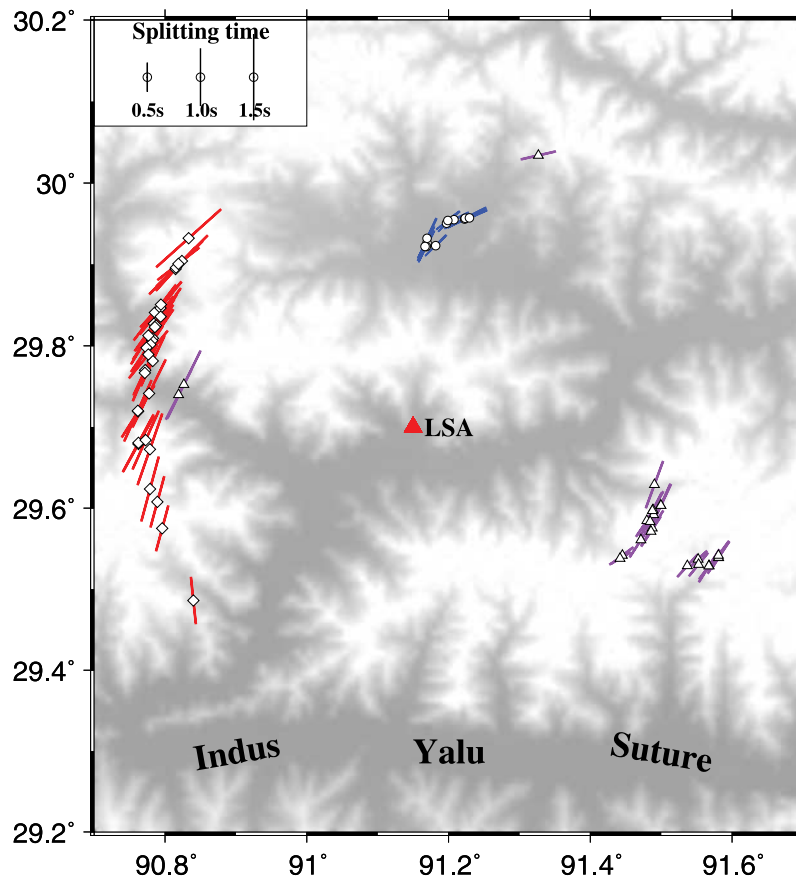


**Figure 2.** Topographic relief map showing shear wave splitting measurements using PKS (blue bars with circles), SKKS (red bars with diamonds), and SKS (purple bars with triangles) plotted on top of ray-piercing points at 200 km depth. Note systematic variations of the splitting parameters with azimuth.

for station SHIO, which is located about 250 km south of the Himalayan front. *Ramesh et al.* [1996] found significant splitting times (about 1 s) at several stations in India, including permanent station HYB which is in southern India. However, subsequent studies using data from HYB and SHIO concluded that the Indian continent is isotropic [*Chen and Ozalaybey*, 1998; *Barruol and Hoffmann*, 1999], as suggested by the overwhelmingly null measurements, which are diagnosed by the lack of observable energy on the transverse component from events with a broad range of back azimuth (BAZ). Recently, using data from several portable seismic experiments, *Singh et al.* [2006, 2007] suggested significant azimuthal anisotropy beneath NE India and in the transitional region between India and Tibet.

[5] Relative to India, results regarding the anisotropy properties on the Lhasa Terrane was less controversial: it has been generally accepted that the mantle beneath the Lhasa Terrane is isotropic or weakly anisotropic, especially beneath the southern

part of the Lhasa Terrane [*Yin and Harrison*, 2000]. *McNamara et al.* [1994] reported a null measurement for a portable station (LHSA). In 1992 the station became a permanent station and was renamed as LSA) in the city of Lhasa which is about 50 km north of the IYS (Figure 1). Significant anisotropy with an E-W fast direction and a splitting time of 1.3 s were found by *McNamara et al.* [1994] at a station (XIGA) approximately 200 km to the SW of LHSA, using an SKS event and an S event. A reassessment of the data by *Sandvol et al.* [1997], however, found no convincing evidence for anisotropy at XIGA. A sharp increase in splitting times north of the BNS was reported [*McNamara et al.*, 1994]. On the basis of SKS data from eight events, *Iidaka and Niu* [2001] found a  $\phi$  of  $70 \pm 8^\circ$  and a  $\delta t$  of  $0.2 \pm 0.1$  s for LSA.

[6] Weak anisotropy with a splitting time of 0.5 s or less was reported by *Hirn et al.* [1995] in the southern part of the Lhasa Terrane and the Himalayan orogenic belts. In the northern part of the

Lhasa Terrane, the splitting times are slightly larger. As discussed by *Sandvol et al.* [1997], the results of *Hirn et al.* [1995] were highly uncertain due to the very small splitting times and the fact that only one event was used. On the basis of a much larger data set (INDEPTH-II), *Sandvol et al.* [1997] concluded that the majority of the stations in the southern part of the Lhasa Terrane show no evidence of anisotropy, and the northern part is weakly anisotropic. This conclusion was re-enhanced by *Huang et al.* [2000] using data from the INDEPTH-III experiment. While splitting times of larger than 1.2 s were commonly observed north of ST17 (which was located about 40 km south of the surface expression of the BNS), all the stations south of this location show negligible splitting times. The conclusion that the southern Lhasa Terrane is nearly isotropic is consistent with a more recent study of *Fu et al.* [2008].

[7] Although significant anisotropy was found at most of the portable seismic stations on the eastern margin of the Tibetan Plateau [*Flesch et al.*, 2005; *Lev et al.*, 2006; *Sol et al.*, 2007], the conclusion that the majority of India and southern Tibet are weakly anisotropic has been widely accepted and has been used in a variety of ways, including constructing geodynamic models [e.g., *Davis et al.*, 1997; *Holt et al.*, 2000; *Flesch et al.*, 2005] and comparing with gravity anomalies [*Chen and Ozalaybey*, 1998]. Here we show that at least in the vicinity of station LSA, the Earth's crust and mantle are highly anisotropic with a splitting time that is greater than the global average.

### 3. Data and Method

[8] The seismograms used in the study were recorded by the New China Digital Seismograph Network station LSA (latitude 29.70°, longitude 91.13°, elevation 3.66 km) over a 15+ year period from 01/1992 to 10/2007. LSA is the only broadband seismic station that recorded 3 or more years of data on the Lhasa Terrane. As demonstrated below, a long recording time is essential in order to reveal significant azimuthal variations of the splitting parameters.

[9] In this study we use three P-to-S converted phases at the core-mantle boundary on the receiver side, including PKS, SKKS, and SKS. The epicentral distance range used is 120°–180° for PKS and 84°–180° for SKKS and SKS. For PKS and SKKS, the cutoff magnitude is 5.8 for shallower (focal depth  $\leq$  100 km) and 5.7 for deeper events,

and for SKS, the cutoff magnitude is 5.6 for shallower and 5.5 for deeper events. The number of three-component seismograms obtained from the Incorporated Research Institutions for Seismology (IRIS) Data Management Center (DMC) is about 620 for PKS, 1350 for SKKS, and 2160 for SKS.

[10] The seismograms were band-pass filtered in the frequency range of 0.04–0.5 Hz to improve signal-to-noise ratio (S/N). An automatic data selection routine was then applied to reject events with low S/N on the radial component. The resulting number of usable events is 250 for PKS, 450 for SKKS, and 1180 for SKS. We have visually checked the results of the automatic selection to make sure that no high-quality events were rejected.

[11] The remaining seismograms are then used to search for the optimal pair of XKS splitting parameters ( $\phi$  and  $\delta t$ ), which correspond to the ones that minimize the energy on the corrected transverse component [*Silver and Chan*, 1991]. The errors in the resulting splitting parameters are calculated using the inverse  $F$  test and represent the 95% confidence level (and are thus approximately 2 standard deviations) [*Silver and Chan*, 1991].

[12] The XKS time window used to compute the splitting parameters is initially set as  $a = 5$  s before and  $f = 20$  s after the predicted arrival times based on the IASP91 earth model. We visually check each of the seismograms to adjust the  $a$  and  $f$  values and to reject the ones with strong non-XKS arrivals in the XKS window. Figures 3–5 show examples of the original and corrected components as well as particle motion diagrams. The resulting measurements were ranked in to A (outstanding), B (good), C (poor), and N (null) based on the S/N on the original and corrected radial and transverse components [*Liu et al.*, 2008]. The null measurements are characterized by a paucity of observable XKS energy on the transverse component.

[13] For a one-layer model of anisotropy (regardless the degree of anisotropy as long as it is not zero), energy on the transverse component can always be observed if the seismogram is noise-free, even when the back azimuth coincides “exactly” with the fast or slow direction. This is because source-side scattering and the finite dimensions of the focal plane always produce arrivals that are not exactly from the fast or slow directions.

[14] We compute synthetic seismograms based on the formalism of *Silver and Chan* [1991] to investigate the effect of a number of factors on the

Station: LSA; Baz= 4.954 deg., Dist= 135.451 deg.  
EQ000722221; Ev-lat= 14.975; Ev-lon= -92.444; Ev-Dep= 62.0km

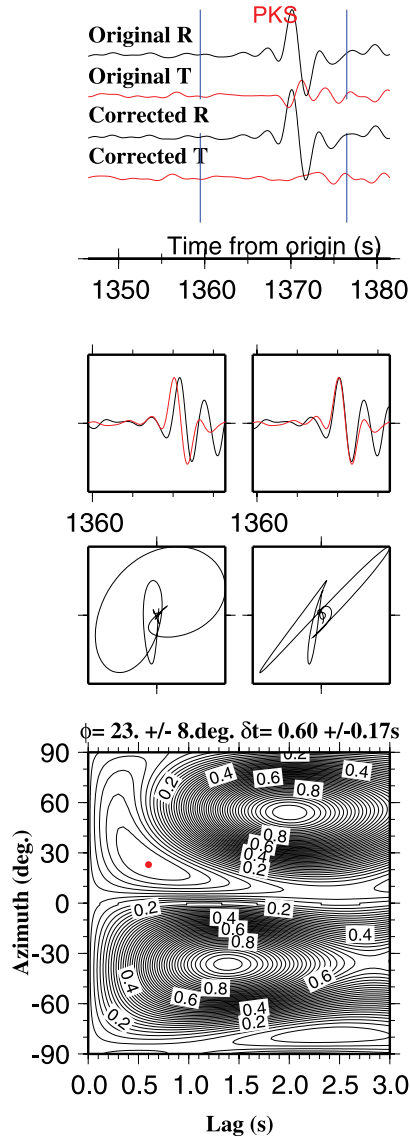


**Figure 3.** Original and corrected radial and transverse components, their particle motion patterns and the error function for a PKS event.

amplitude of transverse XKS arrivals. A Gaussian function, a decaying sinusoid, and a realistic XKS arrival were used as the incoming, presplit, waveform. Some main conclusions from the synthetic tests include:

[15] 1. A dominant period ( $T$ ) that is closer to  $2 \cdot \delta t$  results in larger transverse energy. This explains the fact that larger ( $>7.0$ ) and/or shallower events, which produce longer-period ( $>10$  s) waveforms, are more likely generating null measurements than smaller/deeper events.

[16] 2. Similarly, a  $\delta t$  that is closer to  $T/2$  leads to more observable transverse energy. When  $\delta t$  is 1 s or less, the maximum transverse amplitude is less than half of the maximum radial energy, and when  $\delta t$  is 0.5 s or less, the transverse/radial amplitude ratio is about 1/4 or less.

[17] 3. Transverse amplitude is the largest when the difference between the fast and radial component is  $45^\circ$ .

Station: LSA; Baz= 306.271 deg., Dist= 155.577 deg.

**EQ973322253; Ev-lat= -13.740; Ev-lon= -68.788; Ev-Dep=586.0km**

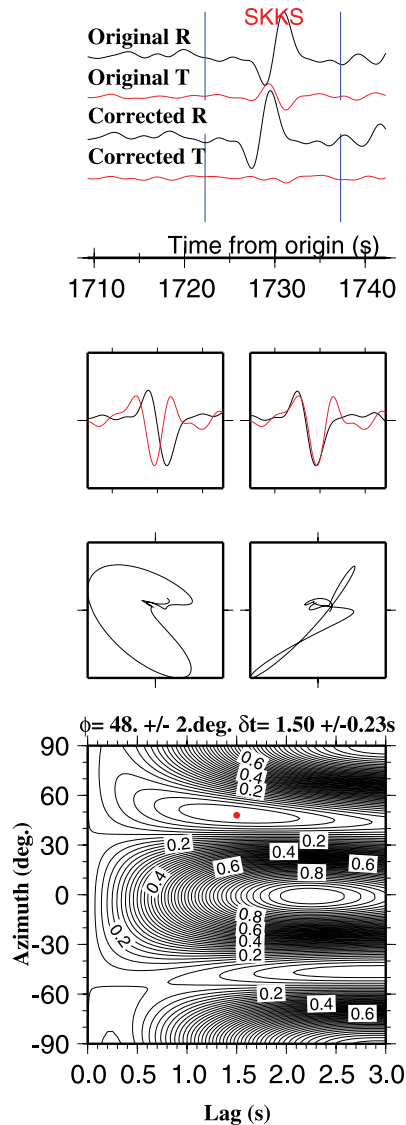


**Figure 4.** Same as Figure 3 but for an SKKS event.

[18] Other factors affecting the S/N on the transverse component (and thus determining whether a particular measurement is considered as null or not) include the magnitude, focal mechanisms, and epicentral distance of the earthquake, ambient noise level at the station, scattering by heterogeneities along the raypath, and filtering parameters, etc.

[19] We performed similar synthetic tests for models with two layers of anisotropy and found that when the splitting time of the lower layer is small (e.g., <1 s as what we found beneath LSA, see below), the transverse amplitude is approximately proportional to  $\sin(2\delta\phi_{12})$  where  $\delta\phi_{12}$  is the differ-

ence between  $\phi_1$  (the fast direction of the lower layer) and  $\phi_2$  (the fast direction of the upper layer). Obviously, a  $\delta\phi_{12}$  of  $45^\circ$  leads to the largest amplitude. A characteristic difference between single and double layers is that the transverse amplitude varies significantly with the back azimuth for a single layer and is less variant for a double layer. This might explain the fact that “null” measurements were suggested by previous studies, on the basis that events from different back azimuths show weak energy on the transverse components. Additionally, similar to the one-layer case, the amplitude of the transverse component increases

Station: LSA; Baz= 279.167 deg., Dist= 105.608 deg.

EQ973141247; Ev-lat= 0.050; Ev-lon= -16.893; Ev-Dep= 10.0km

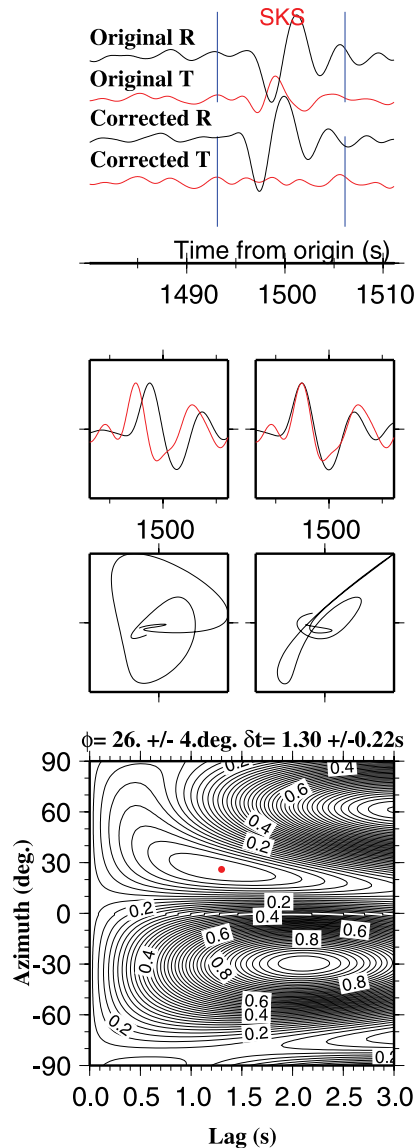


**Figure 5.** Same as Figure 3 but for an SKS event.

with a decreasing difference between  $T$  and  $2\delta t_2$ , which is the splitting time of the upper layer.

[20] The synthetic tests suggest that pure null measurements above an area of anisotropy (regardless the number of layers) are nonexistent for noise-free seismograms, and consequently, for a realistic transverse seismogram with noise, whether the measurement is null or not is highly subjective, and is heavily dependent on the observer's criteria about what a null measurement is. For those reasons, only seismograms with clearly observable

XKS energy on the transverse component are used in the study.

#### 4. XKS Splitting Measurements

[21] A total of 67 quality A or B measurements are obtained, among which 11 are PKS, 32 are SKKS, and 24 are SKS measurements (Table 1). Those measurements were obtained from the approximately 4100 three-component seismograms that we requested from the IRIS DMC and represent a mere 1.6% rate of success.

**Table 1.** Shear Wave Splitting Measurements

Origin Time	Phase	$\phi$ (deg)	$\delta t$ (s)	BAZ (deg)	$\Delta$ (deg)	RP (s/deg)	$m_b$	Dep (km)	Rank
1992-107-1833	SKKS	42 ± 4	1.05 ± 0.20	293.0	159.2	5.23	5.8	122	B
1992-317-2228	SKS	34 ± 2	0.65 ± 0.10	109.3	101.4	4.75	5.9	359	B
1993-074-1608	SKKS	26 ± 3	1.30 ± 0.18	276.3	163.9	5.08	6.2	28	A
1993-143-0659	SKS	34 ± 3	0.65 ± 0.15	110.5	86.8	6.17	5.7	177	B
1993-303-1759	SKKS	15 ± 5	1.15 ± 0.20	258.4	162.2	5.13	6.3	107	B
1993-318-0159	SKKS	31 ± 4	1.35 ± 0.28	286.6	160.5	5.19	5.8	112	B
1994-054-1413	PKS	45 ± 16	0.40 ± 0.17	10.7	131.9	3.50	5.8	73	B
1994-073-2051	PKS	25 ± 6	0.75 ± 0.18	4.8	134.4	3.20	5.8	164	B
1994-300-2220	SKS	33 ± 2	0.70 ± 0.10	113.4	100.9	4.76	6.7	518	A
1994-346-0741	SKKS	45 ± 2	1.30 ± 0.18	300.4	158.6	5.25	6.3	148	A
1995-045-1553	SKKS	39 ± 4	1.05 ± 0.20	283.5	160.1	5.20	6.0	147	B
1995-228-1504	SKS	60 ± 10	0.40 ± 0.08	119.0	103.7	4.55	5.7	463	B
1995-255-1423	SKS	35 ± 10	0.60 ± 0.20	109.2	100.0	4.81	5.6	599	B
1995-282-1343	SKS	42 ± 4	0.50 ± 0.12	113.8	91.4	5.70	6.3	104	B
1996-299-1959	SKKS	52 ± 16	0.90 ± 0.35	301.2	158.8	5.24	5.7	116	B
1997-080-1207	SKS	53 ± 12	0.45 ± 0.15	118.2	103.5	4.56	6.3	448	B
1997-314-1247	SKS	26 ± 4	1.30 ± 0.22	279.2	105.6	4.46	5.6	10	B
1997-332-2253	SKKS	48 ± 2	1.50 ± 0.23	306.3	155.6	5.31	6.7	586	B
1997-359-2216	PKS	26 ± 12	0.60 ± 0.20	4.8	136.3	3.06	5.8	10	B
1998-348-1625	SKKS	174 ± 6	0.80 ± 0.15	235.4	163.0	5.10	6.0	138	B
1999-002-1927	SKS	36 ± 6	0.60 ± 0.13	110.2	86.8	6.16	5.7	226	B
1999-061-1745	SKKS	34 ± 4	1.30 ± 0.20	286.1	160.5	5.19	5.9	110	B
1999-125-2241	PKS	45 ± 6	0.50 ± 0.10	8.1	135.8	3.10	6.3	33	B
1999-128-2212	PKS	28 ± 10	0.55 ± 0.12	4.3	136.2	3.06	6.1	39	B
1999-166-2042	PKS	52 ± 4	0.50 ± 0.05	10.9	131.5	3.55	7.0	70	B
1999-172-1743	PKS	63 ± 12	0.80 ± 0.22	16.0	130.7	3.66	6.3	68	B
1999-237-0706	SKS	46 ± 10	0.40 ± 0.10	112.1	89.7	5.84	5.7	263	B
1999-258-0301	SKKS	35 ± 6	1.15 ± 0.35	289.2	158.7	5.24	6.4	218	A
1999-261-2351	SKS	39 ± 8	0.50 ± 0.15	112.8	89.8	5.88	5.9	102	B
1999-325-0351	SKKS	35 ± 6	1.10 ± 0.35	289.0	160.3	5.19	6.0	101	B
1999-363-0519	PKS	62 ± 10	0.65 ± 0.15	15.9	130.8	3.64	5.9	69	A
2000-072-2221	PKS	23 ± 8	0.60 ± 0.17	4.9	135.4	3.13	6.3	62	A
2000-114-0927	SKKS	28 ± 13	1.10 ± 0.35	267.1	157.4	5.25	7.0	608	B
2000-114-1701	SKKS	29 ± 5	1.10 ± 0.15	266.9	157.3	5.25	6.1	609	A
2000-125-2036	SKS	24 ± 4	0.80 ± 0.25	105.5	98.9	4.92	6.5	515	B
2000-168-0755	SKKS	15 ± 16	0.80 ± 0.28	250.6	163.5	5.09	6.4	120	B
2000-203-0613	PKS	64 ± 7	0.55 ± 0.10	12.7	131.2	3.58	5.9	80	B
2000-222-1141	PKS	66 ± 7	0.65 ± 0.10	17.2	130.6	3.69	6.5	45	B
2000-246-1702	SKS	31 ± 2	0.55 ± 0.10	107.7	99.4	4.84	6.0	687	B
2000-334-1025	SKKS	25 ± 14	0.95 ± 0.43	282.5	163.3	5.10	6.3	58	B
2001-074-1302	SKKS	15 ± 8	0.90 ± 0.18	255.7	164.9	5.05	6.0	37	B
2001-075-0436	SKKS	38 ± 4	1.15 ± 0.22	292.3	159.6	5.22	5.8	115	B
2001-139-1736	SKS	27 ± 2	0.65 ± 0.12	106.8	100.7	4.80	6.0	368	B
2001-170-0932	SKKS	34 ± 12	0.75 ± 0.25	285.3	160.0	5.20	6.0	146	B
2001-180-1835	SKKS	37 ± 2	1.20 ± 0.18	291.2	157.1	5.29	6.1	273	A
2001-240-0656	SKKS	35 ± 5	1.20 ± 0.30	290.9	161.4	5.16	5.9	65	B
2001-273-1901	SKS	32 ± 6	0.65 ± 0.25	112.3	88.2	6.06	6.2	33	B
2001-275-0048	SKS	20 ± 2	0.85 ± 0.15	101.8	102.1	4.73	6.2	106	B
2001-299-2305	SKS	36 ± 6	0.55 ± 0.15	112.3	88.2	6.06	6.1	33	B
2002-087-0456	SKKS	34 ± 4	1.35 ± 0.27	288.7	159.9	5.21	6.5	125	B
2002-091-1959	SKKS	19 ± 7	1.30 ± 0.35	265.8	164.8	5.05	6.4	71	B
2002-181-2129	SKS	32 ± 4	0.70 ± 0.15	110.3	99.1	4.88	6.5	620	B
2002-251-1315	SKS	33 ± 2	0.60 ± 0.07	111.0	99.2	4.88	6.0	618	B
2003-016-0053	SKS	77 ± 8	0.60 ± 0.10	27.9	97.7	5.12	6.3	10	B
2003-095-2203	SKS	32 ± 4	0.45 ± 0.15	110.5	86.8	6.17	5.9	177	B
2003-226-1823	SKS	29 ± 1	0.75 ± 0.08	107.0	100.3	4.80	5.9	563	B
2003-288-0219	SKS	25 ± 4	0.80 ± 0.22	105.5	98.8	4.92	6.0	582	B
2004-027-1600	SKKS	45 ± 3	1.25 ± 0.25	302.1	159.9	5.21	5.8	56	B
2004-035-0518	SKKS	32 ± 4	1.05 ± 0.13	272.9	157.3	5.26	5.8	558	B
2004-077-0321	SKKS	31 ± 8	1.15 ± 0.40	286.8	157.4	5.28	6.1	289	B
2005-106-2241	SKKS	42 ± 2	1.00 ± 0.12	300.1	158.8	5.24	5.8	118	A
2006-237-0044	SKKS	23 ± 8	1.05 ± 0.38	280.0	159.9	5.20	6.6	184	B

**Table 1.** (continued)

Origin Time	Phase	$\phi$ (deg)	$\delta t$ (s)	BAZ (deg)	$\Delta$ (deg)	RP (s/deg)	$m_b$	Dep (km)	Rank
2006-255-1330	SKKS	$24 \pm 4$	$1.10 \pm 0.12$	267.5	162.6	5.12	6.0	114	B
2006-317-0126	SKKS	$24 \pm 2$	$1.15 \pm 0.15$	272.9	157.1	5.26	6.8	572	B
2007-124-1206	SKS	$27 \pm 16$	$0.95 \pm 0.33$	276.8	104.6	4.54	6.2	10	B
2007-145-1747	SKKS	$25 \pm 3$	$0.95 \pm 0.18$	280.5	159.8	5.21	5.9	180	A
2007-202-1534	SKKS	$28 \pm 14$	$0.75 \pm 0.38$	284.5	157.9	5.26	6.4	289	B

[22] Several factors contributed to this apparent low rate. First of all, in order to include all the possibly usable events, cutoff magnitudes that are lower than most previous studies were used for data request. This led to a large number of low S/N seismograms that were rejected by the automated data selection procedure. Second, the maximum epicentral distance used for data request is  $180^\circ$  rather than the  $120\text{--}140^\circ$  used by most previous studies. About 1/2 of all the requested events have an epicentral distance of  $130^\circ$  or greater and thus have lower S/N than closer events. Third, about 3/4 of the requested data are from shallow (focal depth  $\leq 70$  km) events which have complicated waveforms that are not ideal to produce well-defined splitting parameters. Similarly, large ( $m_b \geq 7.1$ ) events, regardless of the focal depth, tend to produce complicated and long-period waveforms and are thus also less capable in producing well-defined measurements. As a matter of fact, none of the  $\sim 110$  seismograms from magnitude  $\geq 7.1$  events produced a quality A or B measurement. Finally, the anticipated complicated crustal and mantle structure as well as large surface relief in the vicinity of the station cause strong scattering of the incoming seismic waves, as evidenced by strong non-XKS arrivals following the initial XKS arrival. Consequently, a XKS window that ends within a few seconds after the initial onset of the XKS arrival must be used for most measurements in order to minimize the influence of the late-arriving scattered waves. This procedure requires a sharp and high S/N XKS waveform. In spite of those factors, on average there are about four well-defined measurements per year, which is comparable with the majority of previous shear wave splitting studies.

[23] Using the unbiased estimator of mean and sample standard deviation [Galassi *et al.*, 2007] (see Liu *et al.* [2008] for its application to shear wave splitting result), the resulting averages are ( $33.0 \pm 9.3^\circ$ ,  $0.7 \pm 0.3$  s) for the entire data set.

#### 4.1. PKS Results

[24] All the PKS events are from the Central American subduction zone, with a narrow back

azimuthal range of  $4\text{--}17^\circ$  and an epicentral distance range of  $131\text{--}136^\circ$  (Figure 6). The mean splitting parameters are ( $46.6 \pm 16.3^\circ$ ,  $0.5 \pm 0.1$  s).

#### 4.2. SKKS Results

[25] The epicentral distance of the 32 SKKS event has a range of  $156\text{--}165^\circ$  (Figure 7), and the average splitting parameters are ( $35.3 \pm 10.3^\circ$ ,  $1.1 \pm 0.2$  s). Sandvol *et al.* [1997] analyzed data from the 1993–074 event and obtained a  $\phi$  of  $28 \pm 7^\circ$  and a  $\delta t$  of  $1.2 \pm 0.4$  s, which are consistent with our result of  $26 \pm 3^\circ$  and  $1.30 \pm 0.12$  s for the same event. On the basis that all the SKS phases analyzed by Sandvol *et al.* [1997] show null measurements, the well-defined SKKS event was not considered by the authors as representative in the interpretation of the shear wave splitting measurements.

#### 4.3. SKS Results

[26] Because of the Earth's seismicity pattern, 21 of the 24 SKS events are from the SW Pacific subduction zone, which has a narrow BAZ range to LSA, from  $102^\circ$  to  $119^\circ$ . Within the small range, rapid and systematic azimuthal variations for both  $\phi$  and  $\delta t$  are observed: the  $\phi$  observations increase from  $20 \pm 2^\circ$  to  $60 \pm 10^\circ$ , and the  $\delta t$  values decrease from  $0.85 \pm 0.15$  s to  $0.40 \pm 0.10$  s (Figure 8). The average splitting parameters are ( $30.3 \pm 6.3^\circ$ ,  $0.6 \pm 0.2$  s). The 21 events can be divided into two groups based on the ray parameter. The first group of events have a ray parameter range of  $4.55\text{--}4.92$  s/degree, and that for the second group is  $5.70\text{--}6.17$  s/degree. No systematic variations with ray parameters are observed. The two events from the central Atlantic mid-ocean ridge have a BAZ of  $278^\circ$  and yield the largest  $\delta t$  ( $1.30 \pm 0.22$  s and  $0.95 \pm 0.33$  s). When results from the two events are plotted against the back azimuth (modulo- $90^\circ$ ), they form a systematic azimuthal variation pattern with the rest of the events (Figure 8). The event from the off-shore NW United States region results in the largest  $\phi$  ( $77 \pm 8^\circ$ ). This event also forms a consistent

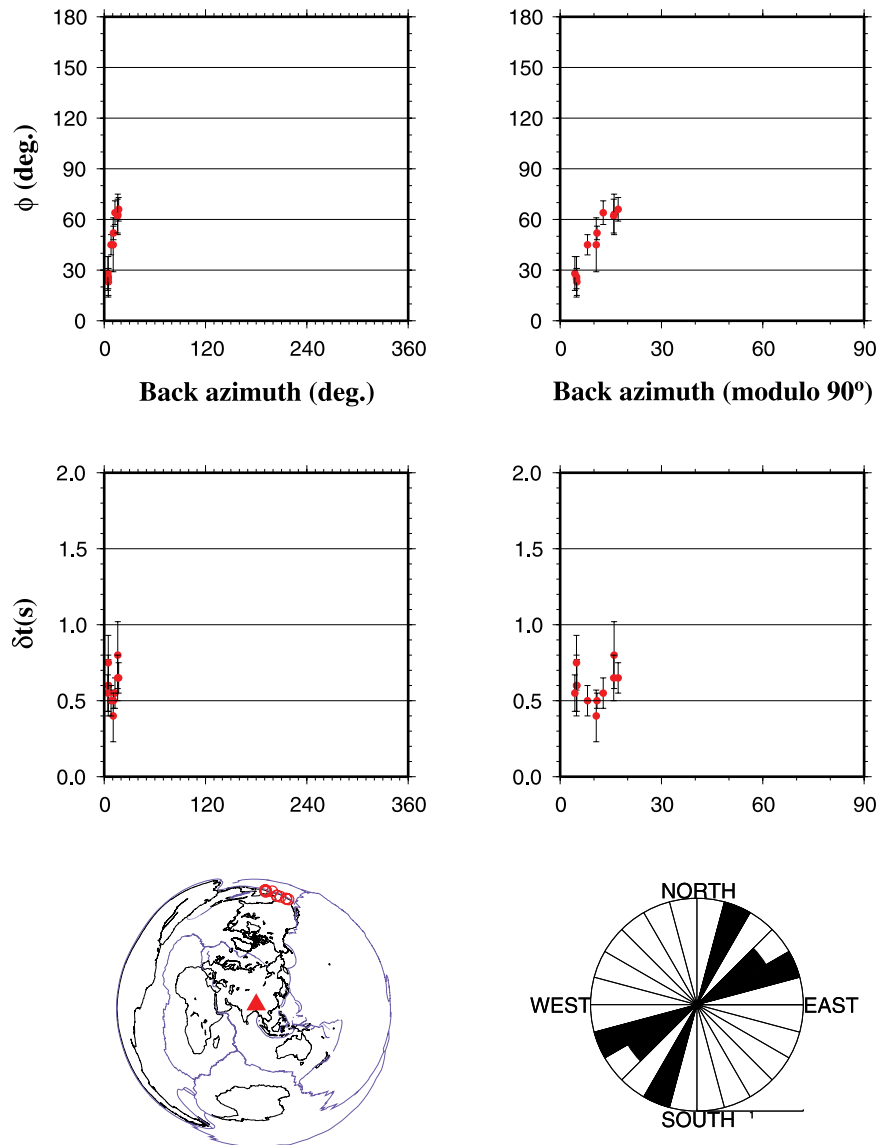


**Figure 6.** Azimuthal variations of (top)  $\phi$  and (middle)  $\delta t$ , (bottom left) distribution of events, and (bottom right) rose diagram of  $\phi$  measurements for the PKS events.

azimuthal variation pattern with the rest of the events (Figure 8).

## 5. Discussion

### 5.1. Fitting With a Two-Layer Model

[27] Given the obvious dependence of the splitting parameters on the back azimuth of the raypath (Figure 9), a model that is more complicated than a single-layer model of anisotropy is required. Consequently, the average splitting parameters cannot correctly represent the anisotropy properties beneath the station. Because the azimuthal variations demonstrate approximately  $\pi/2$  periodicity

(Figure 9), we next try to fit the apparent splitting parameters using a model of two anisotropic layers with horizontal axis of symmetry [Silver and Savage, 1994].

[28] Our attempt to fit all the 67 measurements using a single two-layer model was unsuccessful because of the obvious differences in the azimuthal dependence of the splitting parameters between the three azimuthal groups (Figures 9 and 10). Consequently, we divide the measurements into three groups based on the location of the ray-piercing points and attempt to find the optimal two-layer parameters for each of the groups. The northern group (Figure 10, top) consists of all the 11 PKS

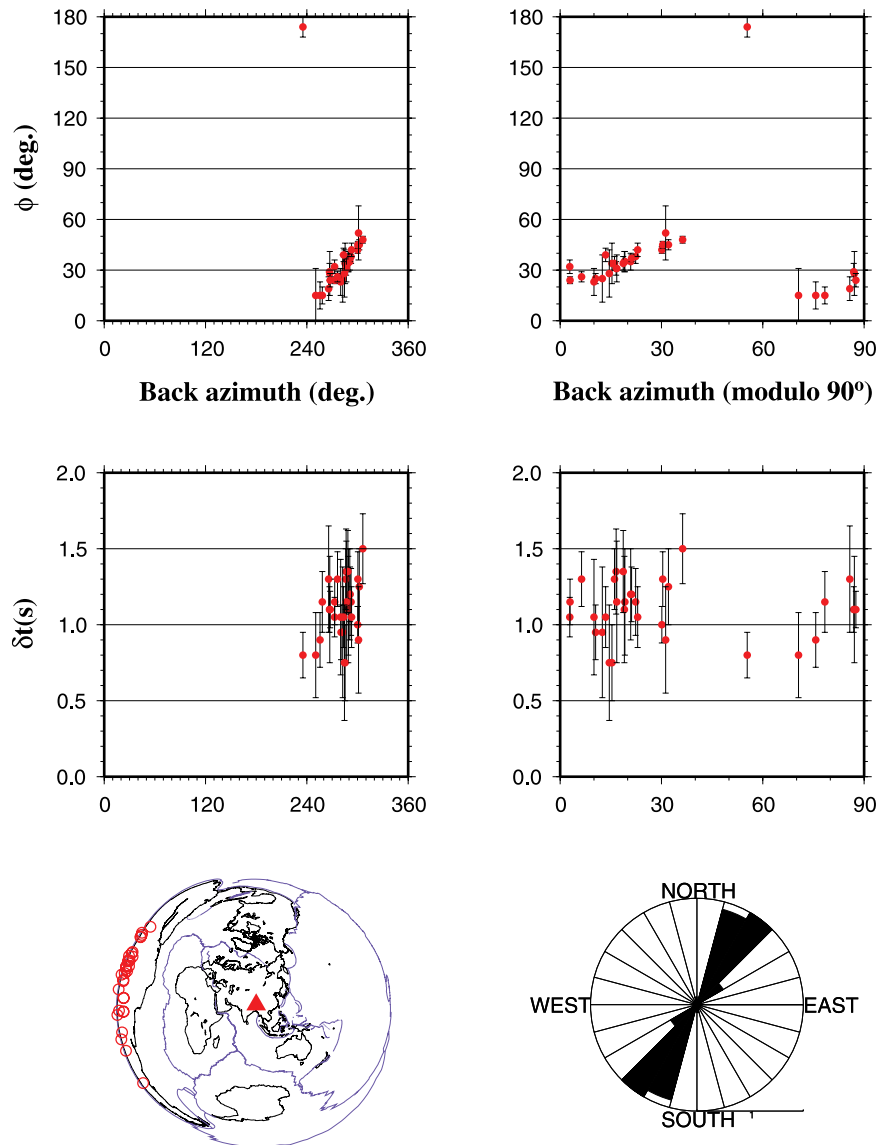


**Figure 7.** Same as Figure 6 but for the SKKS events.

measurements and one SKS measurement. In the small BAZ range of  $4\text{--}17^\circ$ , the  $\phi$  values from the PKS increase by more than  $40^\circ$ , and the  $\delta t$  observations have a “U”-shaped pattern with the minimum value around  $\text{BAZ} = 20^\circ$ . The SE group consists of 21 SKS measurements (Figure 10, middle). Relative to the northern group, the azimuthal variations of  $\phi$  have a smaller slope. The western group consists of all the 32 SKKS and 2 SKS measurements, covering a near- $90^\circ$  azimuthal range (Figure 10, bottom).

[29] In this study we used PKS, SKKS, and SKS phases, which have different peak period due to the

difference in wave type and propagation path. We calculated that the average peak period is  $4.6 \pm 0.8$ ,  $7.6 \pm 0.6$ , and  $5.7 \pm 0.5$  s for PKS, SKKS, and SKS, respectively. Because it is well-known that under a two-layer model, the azimuthal dependence of the apparent splitting parameters (i.e., parameters measured under the assumption of a single layer) is a function of central period, we take the central frequency into consideration when performing the calculation of apparent parameters using the methodology of *Silver and Savage* [1994].

[30] The optimal pairs of parameters are these corresponding to the minimum misfit between the

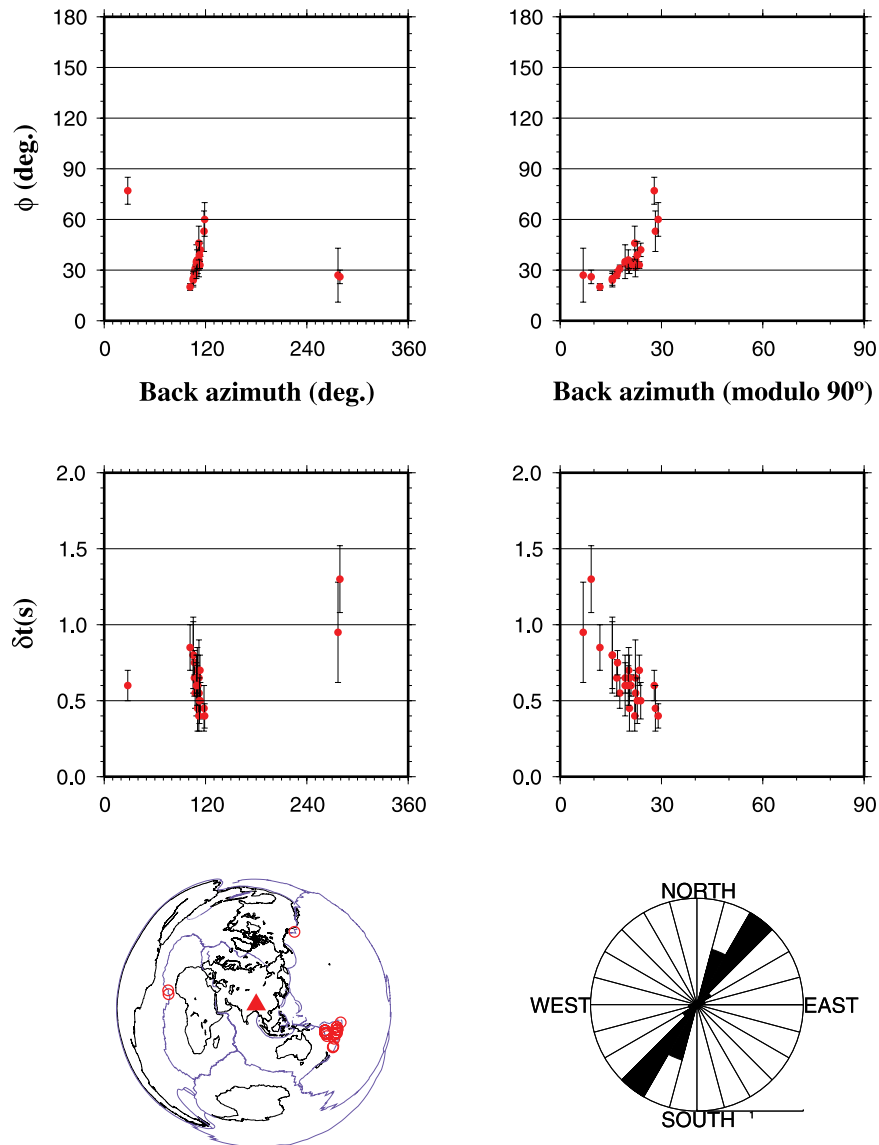


**Figure 8.** Same as Figure 6 but for the SKS events.

calculated and observed splitting parameters. The misfit is defined as

$$\chi^2 = \sum_{i=1}^n w_1 * [(\phi_i^{obs} - \phi_i^{cal}) / \sigma_{\phi_i}]^2 + w_2 * [(\delta t_i^{obs} - \delta t_i^{cal}) / \sigma_{\delta t_i}]^2, \quad (1)$$

where  $\sigma_{\phi_i}$  and  $\sigma_{\delta t_i}$  is the standard deviation of the  $i$ th  $\phi$  and  $\delta t$  measurement, respectively,  $n$  is the number of events,  $w_1 + w_2 = 1$  are the weighting factors for the  $\phi$  and  $\delta t$  observations, respectively. In this study we use  $w_1 = w_2 = 0.5$  to give equal weight on the  $\phi$  and  $\delta t$  measurements. The step width of the grid searching is  $1^\circ$  for  $\phi$  and  $0.05$  s for  $\delta t$ . In order to avoid dominance by observations

with very small errors, a lower limit of  $5^\circ$  is set for  $\sigma_{\phi_i}$ , and of  $0.1$  s is set for  $\sigma_{\delta t_i}$ .

[31] For the northern, SE, and western group, respectively, the best-fitting  $\phi$  for the lower layer is  $-80^\circ$ ,  $-53^\circ$ , and  $-61^\circ$ , and that for the upper layer is  $49^\circ$ ,  $59^\circ$ , and  $40^\circ$ . The corresponding values for  $\delta t$  in the lower layer is  $0.9$ ,  $0.55$ , and  $0.90$  s, and that for the upper layer is  $0.45$ ,  $0.55$ , and  $1.45$  s.

[32] Numerous previous studies suggest that the resulting parameters of the two layers are non-unique, especially when the azimuthal coverage is insufficient. One of the characteristics of such nonuniqueness is that a set of totally different parameters can lead to similar goodness of fit to

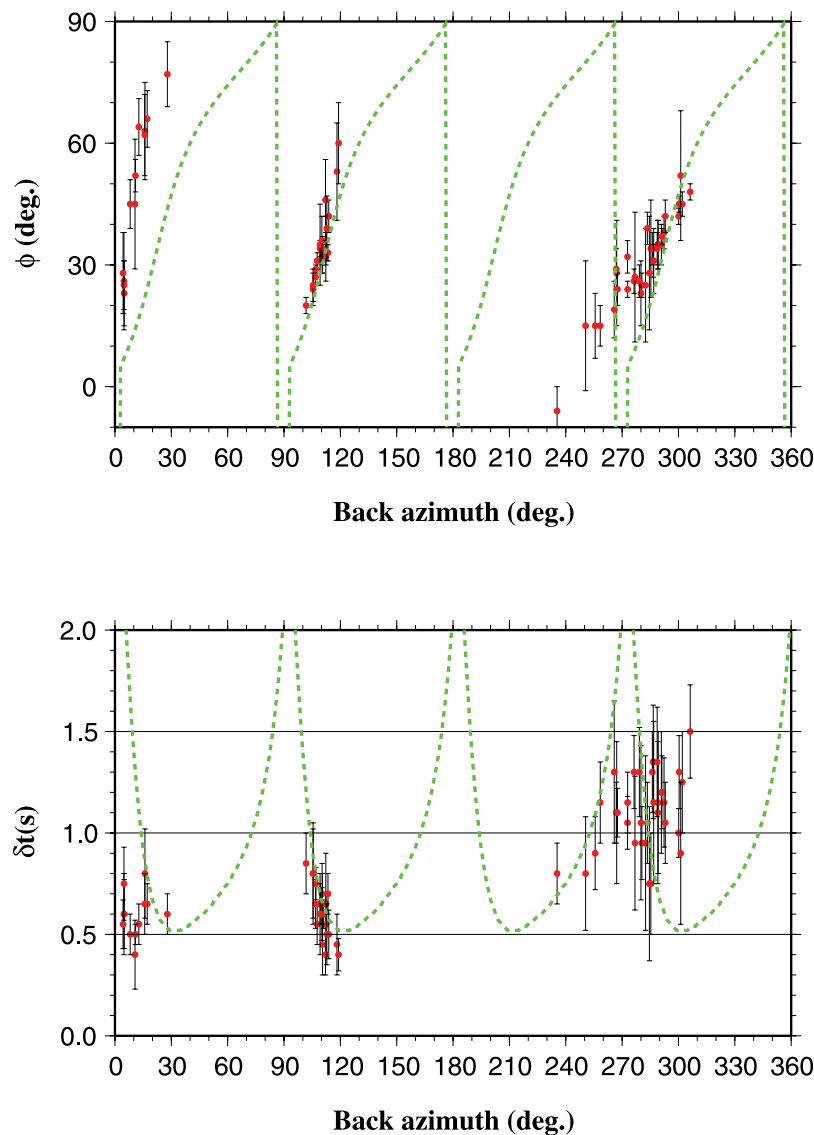


**Figure 9.** XKS splitting parameters plotted against back azimuth of the events, showing possible  $\pi/2$  periodicity. The dashed lines are calculated splitting parameters using a two-layer model of anisotropy with the following parameters: lower layer,  $\phi_1 = -50^\circ$ ,  $\delta t_1 = 0.55$  s; upper layer,  $\phi_2 = 60^\circ$ ,  $\delta t_2 = 0.55$  s. The dominant frequency used in the calculation is 0.2 Hz.

the observed data. We qualitatively estimate the uniqueness by using the “stability” of the resulting parameters as a function of misfit. For each of the three azimuthal groups, we first perform a grid search of the optimal set of the four parameters corresponding to the minimum misfit using equation (1). We then calculate a scaled misfit between the misfit from each of the parameter sets and that from the optimal set, using  $\lambda = 100 * (\chi^2 - \chi_{\min}^2) / \chi_{\min}^2$ , where  $\chi_{\min}^2$  is the minimum misfit. Figure 11 suggests that among the 12 parameters, the splitting times of both the upper and lower layers in the western group are not well-defined, as demonstrated by the large scatter of the plots. This is caused by

the fact that the fast directions of the upper and lower layers for the western group are not far ( $11^\circ$ ) from being orthogonal to each other. For two layers that are perfectly orthogonal to one another, the net splitting time is the difference between the splitting time of the individual layers and thus it is impossible to find the absolute value of the individual times. Consequently, the splitting times of the western group are not used in the discussion below.

## 5.2. Geodynamic Implications

[33] A recent joint analysis of shear wave splitting and GPS observations for the eastern part of the

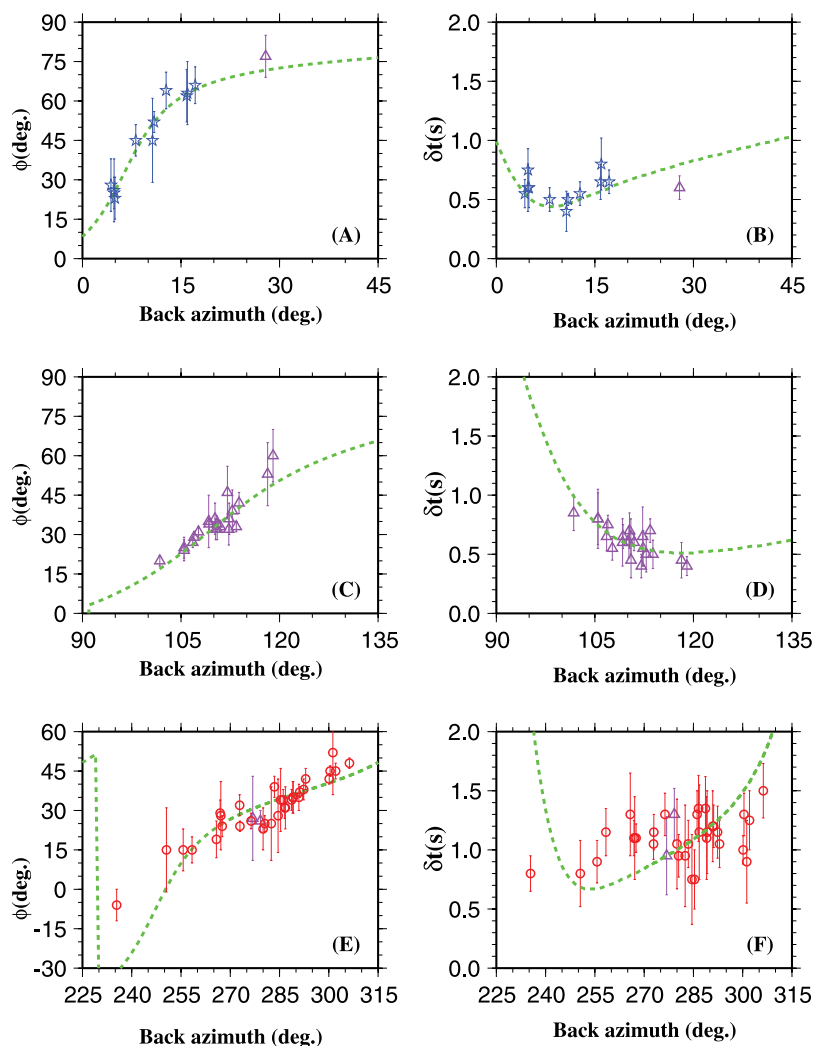


**Figure 10.** Azimuthal variation of splitting parameters for the (top) northern, (middle) southeastern, and (bottom) western event groups. Stars, PKS; circles, SKKS; triangles, SKS. Dashed lines represent calculated splitting parameters computed using the best fitting model and the average period for PKS (northern group), SKS (SE group), and SKKS (western group).

Tibetan Plateau concluded that the crust and lithospheric mantle deform coherently [Wang *et al.*, 2008]. Stations without clear splitting, including LSA at which previous studies suggest null measurements, were not used, and splitting parameters were averaged due to the lack of systematic azimuthal variations. In addition, shear wave splitting measurements in the area south of the BNS is excluded from the modeling because of the possible influence from the Indian lithosphere [Wang *et al.*, 2008].

[34] Our measurements at LSA reveal strong anisotropy which can be satisfactorily explained by a two-layer model, suggesting that the mantle structure and dynamics beneath the southern Lhasa Terrane are different considerably from the eastern

part of the Tibetan Plateau. This is consistent with the suggestion of Wang *et al.* [2008].

[35] Alternatively, the difference in apparent characteristics of seismic anisotropy beneath the Lhasa Terrane and eastern Tibet could be an artifact, probably arising from the fact that the SKS splitting measurements summarized by Wang *et al.* [2008] are mostly from portable seismic stations, while our results for LSA were from a long-running permanent station. The limited recording time (mostly 1–2 years) for the portable stations might prevent the recognition of azimuthal dependence of splitting parameters. In addition, most of the splitting measurements used by Wang *et al.* [2008] were from a number of different studies and for

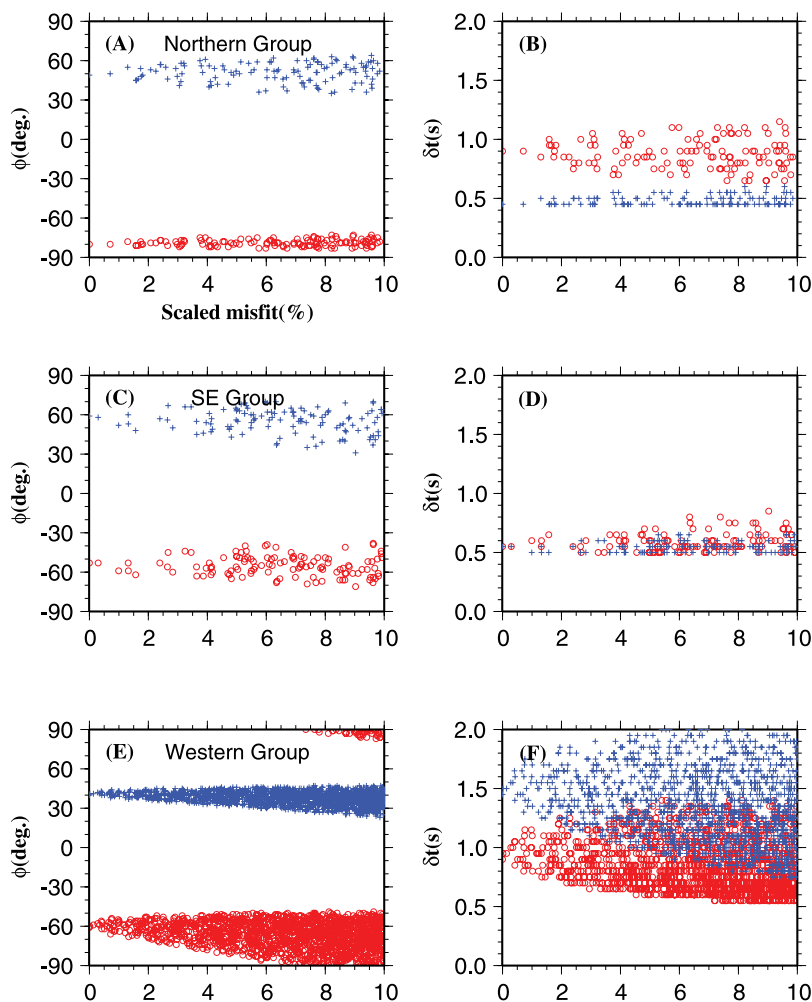


**Figure 11.** Two-layer splitting parameters for the three regions plotted against scaled misfits. Pluses are for the upper layer, and circles are for the lower layer.

most of them, only the SKS phase was used. This might further limit the azimuthal coverage.

### 5.2.1. Models for the Upper Layer of Anisotropy

[36] The fast polarization directions of the upper layer range from  $40^\circ$  to  $59^\circ$ . These are consistent with the surface movement direction revealed by the three GPS measurements in the study area, which suggest a direction of  $45^\circ$  and a velocity of about 25 mm/a relative to the stable interior of Eurasia (Figure 12) [Zhang *et al.*, 2004]. The two well-defined splitting times of the upper layer are 0.45 and 0.55 s, corresponding to a thickness of about 50 km for a layer with 4% anisotropy, 30 km for 7% anisotropy, or 15 km for 15% anisotropy.

[37] A commonly proposed mechanism for crustal anisotropy is preferred alignment of cracks in the upper crust with the fast direction being parallel to

the strike of the cracks [Kaneshima *et al.*, 1988]. This mechanism typically produces a  $\delta t$  of 0.2 s or less due to pressure-induced closure of cracks at depth greater than 10–15 km [Kern, 1990]. The large  $\delta t$  values observed at LSA and the lack of surface structures with a NE-SW strike suggest that aligned cracks in the upper crust are probably not the major cause of the observed anisotropy in the upper layer.

[38] Another possible cause of anisotropy in the upper layer is aligned anisotropic minerals in the middle-lower crust, probably by the northeastward plastic flow which is believed to be responsible for the long-distance transferring of materials away from the collisional zone to the South China Platform [Royden *et al.*, 1997]. Such a flow is evidenced by the seismically revealed low-velocity layer in the middle-lower crust [Kind *et al.*, 1996].

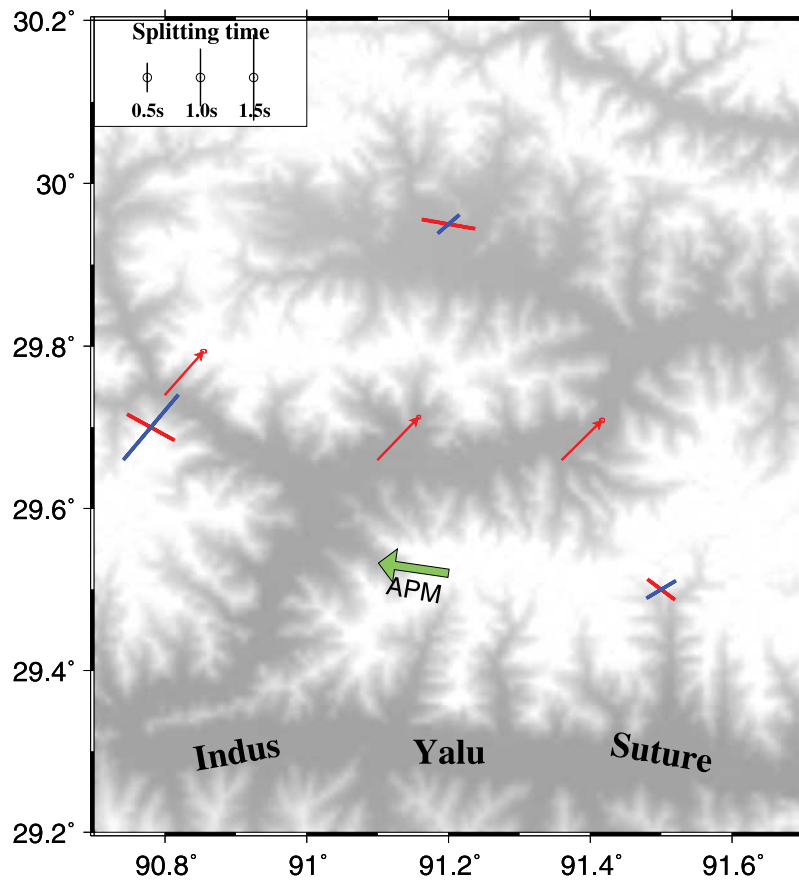


**Figure 12.** Resulting two-layer parameters (red, lower layer; blue, upper layer). Thin arrows are GPS results [Zhang *et al.*, 2004], and the thick arrow is the absolute plate motion direction of Eurasia [Gripp and Gordon, 2002].

[39] Recent laboratory studies of seismic anisotropy of lower-crustal minerals suggest that amphibole, which is a major constituent mineral of the continental middle and lower crust [Rudnick and Gao, 2003], is capable of producing large shear wave anisotropy (up to 30% [Tatham *et al.*, 2008]) with the fast polarization direction being subparallel to the flow direction [Tatham *et al.*, 2008; Aspiroz *et al.*, 2007]. A  $\delta t$  of 0.5 s requires a layer with an anisotropy of 10% and a thickness of 20 km, which is comparable with the thickness of the seismically revealed middle-lower crustal low-velocity layer beneath the southern Lhasa Terrane [Kind *et al.*, 1996]. Under high strain, lower crustal schists are found to have an anisotropy of as large as 35% [Okaya *et al.*, 1995], suggesting that a layer in the middle-lower crust as thin as 5 km is sufficient to produce the observed  $\delta t$  for the upper layer.

[40] If the middle-lower crust is indeed anisotropic with a splitting time of  $\sim 0.5$  s, in principle splitting of the P-to-S converted phase from the Moho should be observed [McNamara and Owens, 1993; Peng

and Humphreys, 1997], although ambiguities in the interpretation of the resulting splitting parameters do exist [Savage, 1999]. To search for evidences of splitting in P-to-S converted waves from the Moho, we requested from the IRIS DMC all the teleseismic *P* wave data recorded by LSA for earthquakes in the epicentral distance range of 40–90°, magnitude  $\geq 5.6$ , and focal depth  $\geq 300$  km, and computed radial and transverse receiver functions using the time domain deconvolution procedure of Ammon *et al.* [1990]. Although significant energy is observed on the transverse receiver functions, which may suggest crustal anisotropy, a reliable determination of crustal splitting parameters using the receiver functions cannot be obtained. This is probably due to the blurring of the Moho, complex crustal layering, lateral heterogeneities in the crust, and interference of surface topography, all of which are possible in an area with greatly thickened and actively deforming crust such as the Tibetan Plateau. Thus the failure of obtaining reliable crustal splitting parameters from receiver functions is

insufficient to reject the possibility of an anisotropic crust.

[41] It must be mentioned that the upper layer of anisotropy can also reside in the subcrustal lithosphere. This model, however, is not favored because there is a lack of known mechanism that could explain the observed NE fast directions if the source of anisotropy is in the subcrustal lithosphere.

### 5.2.2. Models for the Lower Layer of Anisotropy

[42] The fast directions for the lower layer range from  $-53^\circ$  to  $-80^\circ$ , which are approximately consistent with the absolute plate motion direction of Eurasia, and is also subparallel to the strike of the collisional front (Figure 12). The splitting times of the lower layer (0.55–0.90 s) require a layer of 80–130 km thick with 3% anisotropy.

[43] The simplest explanation for the observed anisotropy for the lower layer is that it is caused by the India-Eurasia continental collision which has an approximately N-S shortening direction. Numerous studies show that the fast directions are usually parallel to the strike of collisional mountain belts [Silver, 1996] and is generally considered as the result of A-type LPO of dry olivine which is the major constituent mineral in the mantle [Zhang and Karato, 1995]. The shortening is consistent with the results of a recent study using gravity and geoid data which suggest a doubling of lithosphere thickness beneath the Lhasa Terrane [Jimenez-Munt *et al.*, 2008].

[44] Alternatively, the anisotropy in the lower layer could be caused by mantle flow in the asthenosphere related to the APM of the Eurasian plate, which is moving at a rate of 2.3 cm/a with an azimuth of  $-82^\circ$  at LSA [Gripp and Gordon, 2002]. Such a correlation between  $\phi$  and APM directions has been proposed by Vinnik *et al.* [1992] and others.

[45] It must be mentioned that because there is basically no control on the depth of the anisotropic layers, other possible models for the observed upper and lower layers of anisotropy exist. Examples of such models include asthenospheric flow around the keel of the Indian continent, as suggested for North America [e.g. Fouch *et al.*, 2000; Gao *et al.*, 2008]; small-scale mantle convection as suggested beneath Tienshan [Makeyeva *et al.*, 1992], the Baikal rift zone [Gao *et al.*, 1994], and the western United States [Liu *et al.*, 1995;

Savage and Sheehan, 2000]; and preferred alignment of magmatic dykes in the lithosphere [Gao *et al.*, 1997, 2008; Kendall *et al.*, 2005]. The models proposed here for the southern Lhasa Terrane are the physically most viable ones, on the basis of currently available knowledge on the formation mechanism of seismic anisotropy and that on the structure and dynamics of the southern Lhasa Terrane.

### 5.3. Effect of Length of Recording

[46] It has long been realized that in areas with complex anisotropy, the splitting parameters vary as a function of the back azimuth [Silver and Savage, 1994]. For most cases, such variations are usually large, e.g., up to  $60^\circ$  for the fast direction and 1 s for splitting times at LSA. Obviously, averaged splitting parameters over all the events from a station are heavily biased toward the most populous azimuthal group of events and are thus not representative of the actual anisotropy structure. Because of the uneven distribution of Earth's seismicity, for most locations on Earth a reasonable azimuthal coverage can only be achieved after several years of continuous recording and/or when PKS and SKKS in addition to SKS phases are used. In some areas even a moderately broad azimuthal coverage may never be possible.

[47] Unfortunately, most previous shear wave splitting studies use data from portable seismic experiments (which typically have a duration of 1–2 years), and for most cases, only the SKS phase is used. Consequently, the results were presented in the form of averaged splitting parameters. Such a practice is valid for areas with known simple (single layer with a horizontal axis of symmetry) anisotropy. The problem, however, is that complex anisotropy cannot be recognized until a reasonable azimuthal coverage is obtained.

[48] One of the practices to diagnose complex anisotropy is that in addition to SKS, other P-to-S converted phases such as PKS and SKKS should be used. Note that reliable splitting parameters can still be obtained for events in the range of  $140^\circ$ – $180^\circ$  which is a range usually excluded by most previous studies. Another beneficial practice is that the results should be presented in the form of individual measurements in addition to averaged values, even for data recorded over a short duration. With additional results from future studies in the same area, a reasonable azimuthal coverage is likely to be obtained. Finally, great caution must be

taken for the end users of the splitting measurements, especially when the measurements have a limited azimuthal coverage.

## 6. Conclusions

[49] The most robust conclusion from this study is that contradictory to previous suggestions, the mantle beneath the southern Lhasa Terrane is highly anisotropic with a maximum splitting time of about 1.5 s, which is 50% greater than the global average for continents [Silver, 1996]. In addition, the splitting parameters demonstrate azimuthal dependence and can be satisfactorily explained by two-layer models of anisotropy with horizontal axes of symmetry.

[50] The existence of significant anisotropy beneath the southern Lhasa Terrane provides new constraints on models about crustal and mantle structure of the study area and provides first-hand observations on crustal and mantle deformation associated with continental collision. Unfortunately, owing to the lack of long-running seismic stations in other locations on the Lhasa Terrane, the spatial extent of such significant anisotropy cannot be determined until many years from now when a permanent seismic array is established and after a sufficient amount of data are recorded. The two-layer model established based on data from station LSA can then be tested using the additional data.

## Acknowledgments

[51] Data used in the study were archived and managed by the IRIS DMC. Communications with G. Lloyd clarified the relationship between amphibole LPO and crustal plastic flow. We thank P. Davis and V. Levin for constructive reviews. The study was partially funded by the U.S. National Science Foundation under awards EAR 0440320 and EAR 0739015. This paper is Missouri University of Science and Technology Geology and Geophysics contribution 13.

## References

- Ammon, C. J., G. E. Randall, and G. Zandt (1990), On the nonuniqueness of receiver function inversions, *J. Geophys. Res.*, *95*, 15,303–15,318.
- Aspiroz, M. D., G. E. Lloyd, and C. Fernandez (2007), Development of lattice preferred orientation in clinoamphibles deformed under low-pressure metamorphic conditions. A SEM/EBSD study of metabasites from the Aracena metamorphic belt (SW Spain), *J. Struct. Geol.*, *29*, 629–645.
- Barruol, G., and R. Hoffmann (1999), Upper mantle anisotropy beneath the Geoscope stations, *J. Geophys. Res.*, *104*, 10,757–10,773.
- Chen, W.-P., and S. Ozalaybey (1998), Correlation between seismic anisotropy and Bouguer gravity anomalies in Tibet and its implications for lithospheric structures, *Geophys. J. Int.*, *135*, 93–101.
- Davis, P., P. England, and G. Houseman (1997), Comparison of shear wave splitting and finite strain from the India-Asia collision zone, *J. Geophys. Res.*, *102*, 27,511–27,522.
- Flesch, L. M., W. E. Holt, P. G. Silver, M. Stephenson, C. Y. Wang, and W. W. Chan (2005), Constraining the extent of crust-mantle coupling in central Asia using GPS, geologic, and shear wave splitting data, *Earth Planet. Sci. Lett.*, *238*, 248–268.
- Fouch, M. J., and S. Rondenay (2006), Seismic anisotropy beneath stable continental interiors, *Phys. Earth Planet. Int.*, *158*, 292–320, doi:10.1016/j.pepi.2006.01.022.
- Fouch, M. J., K. M. Fischer, E. M. Parmentier, M. E. Wyssession, and T. J. Clarke (2000), Shear wave splitting, continental keels, and patterns of mantle flow, *J. Geophys. Res.*, *105*, 6255–6275.
- Fu, Y. V., Y. J. Chen, A. Li, S. Zhou, X. Liang, G. Ye, G. Jin, M. Jiang, and J. Ning (2008), Indian mantle corner flow at southern Tibet revealed by shear-wave splitting measurements, *Geophys. Res. Lett.*, *35*, L02308, doi:10.1029/2007GL031753.
- Galassi, M., J. Davies, J. Theiler, B. Gough, G. Jungman, M. Booth, and F. Rossi (2007), GNU scientific library reference manual, Free Software Found., Boston, Mass. (Available at <http://www.gnu.org/software/gsl/>)
- Gao, S., P. M. Davis, H. Liu, P. D. Slack, Y. A. Zorin, V. V. Mordvinova, V. M. Kozhevnikov, and R. P. Meyer (1994), Seismic anisotropy and mantle flow beneath the Baikal rift zone, *Nature*, *371*, 149–151.
- Gao, S. S., P. M. Davis, K. H. Liu, P. D. Slack, A. W. Rigor, Y. A. Zorin, V. V. Mordvinova, V. M. Kozhevnikov, and N. A. Logatchev (1997), SKS splitting beneath continental rift zones, *J. Geophys. Res.*, *102*, 22,781–22,797.
- Gao, S. S., K. H. Liu, R. J. Stern, G. R. Keller, J. P. Hogan, J. Pulliam, and E. Y. Anthony (2008), Characteristics of mantle fabrics beneath the south-central United State: Constraints from shear-wave splitting measurements, *Geosphere*, *4*, 411–417, doi:10.1130/GES00159.
- Gripp, A. E., and R. G. Gordon (2002), Young tracks of hotspots and current plate velocities, *Geophys. J. Int.*, *150*, 321–364.
- Hirn, A., et al. (1995), Seismic anisotropy as an indicator of mantle flow beneath the Himalayas and Tibet, *Nature*, *375*, 571–574.
- Holt, W. E., B. Shen-Tu, J. Ren, N. Chamot-Rooke, X. Le Pichon, and A. J. Haines (2000), Velocity field in Asia inferred from Quaternary fault slip rates and Global Positioning System observations, *J. Geophys. Res.*, *105*, 19,185–19,209.
- Huang, W. C., J. F. Ni, F. Tilmann, D. Nelson, J. Guo, W. Zhao, J. Mechie, R. Kind, J. Saul, R. Rapine, and T. M. Hearn (2000), Seismic polarization anisotropy beneath the central Tibetan Plateau, *J. Geophys. Res.*, *105*, 27,979–27,989.
- Iidaka, T., and F. L. Niu (2001), Mantle and crust anisotropy in the eastern China region inferred from waveform splitting of SKS and PpSms, *Earth Planets Space*, *53*, 159–168.
- Jimenez-Munt, I., M. Fernandez, J. Verges, and J. P. Platt (2008), Lithosphere structure underneath the Tibetan Plateau inferred from elevation, gravity and geoid anomalies, *Earth Planet. Sci. Lett.*, *267*, 276–289, doi:10.1016/j.epsl.2007.11.045.

- Kaneshima, S., M. Adndo, and S. Kimura (1988), Evidence from shear-wave splitting for the restriction of seismic anisotropy to the upper crust, *Nature*, *335*, 627–629.
- Kendall, J.-M., G. W. Stuart, C. J. Ebinger, I. D. Bastow, and D. Keir (2005), Magma-assisted rifting in Ethiopia, *Nature*, *433*, 146–148.
- Kern, H. (1990), Laboratory seismic measurements: An aid in the interpretation of seismic field data, *Terra Nova*, *2*, 617–628.
- Kind, R., J. Ni, W. Zhao, J. Wu, X. Yuan, L. Zhao, E. Sandvol, C. Reese, J. Nabelek, and T. Hearn (1996), Evidence from earthquake data for a partially molten crustal layer in southern Tibet, *Science*, *274*, 1692–1694.
- Lev, E., M. D. Long, and R. D. van der Hilst (2006), Seismic anisotropy in Eastern Tibet from shear wave splitting reveals changes in lithospheric deformation, *Earth Planet. Sci. Lett.*, *251*, 293–304.
- Li, C., R. D. van der Hilst, and M. N. Toksöz (2006), Constraining P-wave velocity variations in the upper mantle beneath Southeast Asia, *Phys. Earth Planet. Inter.*, *154*, 180–195.
- Liu, H., P. M. Davis, and S. Gao (1995), SKS splitting beneath southern California, *Geophys. Res. Lett.*, *22*, 767–770.
- Liu, K. H., S. S. Gao, Y. Gao, and J. Wu (2008), Shear-wave splitting and mantle flow associated with the deflected Pacific slab beneath northeast Asia, *J. Geophys. Res.*, *113*, B01305, doi:10.1029/2007JB005178.
- Mainprice, D., G. Barruol, and W. Ben Ismail (2000), The seismic anisotropy of the Earth's Mantle: From single crystal to polycrystal, in *Earth's Deep Interior: Mineral Physics and Tomography From the Atomic to the Global Scale*, edited by S. I. Karato, pp. 237–264, AGU, Washington, D.C.
- Makeyeva, L. I., L. P. Vinnik, and S. W. Roecker (1992), Shear-wave splitting and small-scale convection in the continental upper mantle, *Nature*, *358*, 144–147.
- McNamara, D. E., and T. J. Owens (1993), Azimuthal shear wave velocity anisotropy in the Basin and Range Province using Moho PS Converted phases, *J. Geophys. Res.*, *98*, 12,003–12,017.
- McNamara, D. E., T. J. Owens, P. G. Silver, and F. T. Wu (1994), Shear wave anisotropy beneath the Tibetan Plateau, *J. Geophys. Res.*, *99*, 13,655–13,665.
- Okaya, D., N. Christensen, D. Stanley, and T. Stern (1995), Crustal anisotropy in the vicinity of the Alpine Fault Zone, *N. Z. J. Geol. Geophys.*, *38*, 579–583.
- Owens, T. J., and G. Zandt (1997), Implications of crustal property variations for models of Tibetan plateau evolution, *Nature*, *387*, 37–43.
- Peng, X., and E. D. Humphreys (1997), Moho dip and crustal anisotropy in northwest Nevada from teleseismic receiver functions, *Bull. Seismol. Soc. Am.*, *87*, 745–754.
- Ramesh, D. S., R. N. Bharthur, K. S. Prakasam, D. Srinagesh, S. S. Rai, and V. K. Gaur (1996), Predominance of plate motion-related strain in the south Indian shield, *Curr. Sci.*, *70*, 843–847.
- Royden, L. H., B. C. Burchfiel, R. W. King, E. Wang, Z. Chen, F. Shen, and Y. Liu (1997), Surface deformation and lower crustal flow in eastern Tibet, *Science*, *276*, 788–790.
- Rudnick, R. L., and S. Gao (2003), The composition of the continental crust, in *The Crust, Treatise on Geochem.*, vol. 3, edited by H. D. Holland and K. K. Turekian, pp. 1–64, Elsevier, New York.
- Sandvol, E. A., J. F. Ni, R. Kind, and W. Zhao (1997), Seismic anisotropy beneath the southern Himalayas-Tibet collision zone, *J. Geophys. Res.*, *102*, 17,813–17,823.
- Savage, M. K. (1999), Seismic anisotropy and mantle deformation: What have we learned from shear wave splitting?, *Rev. Geophys.*, *37*, 65–106.
- Savage, M. K., and A. K. Sheehan (2000), Seismic anisotropy and mantle flow from the Great Basin to the Great Plains, western United States, *J. Geophys. Res.*, *105*, 13,715–13,734.
- Silver, P. G. (1996), Seismic anisotropy beneath the continents - probing the depths of geology, *Annu. Rev. Earth Planet. Sci.*, *24*, 385–432.
- Silver, P. G., and W. W. Chan (1991), Shear wave splitting and subcontinental mantle deformation, *J. Geophys. Res.*, *96*, 16,429–16,454.
- Silver, P. G., and M. Savage (1994), The interpretation of shear-wave splitting parameters in the presence of two anisotropic layers, *Geophys. J. Int.*, *119*, 949–963.
- Singh, A., M. R. Kumar, P. S. Raju, and D. S. Ramesh (2006), Shear wave anisotropy of the northeast Indian lithosphere, *Geophys. Res. Lett.*, *33*, L16302, doi:10.1029/2006GL026106.
- Singh, A., M. R. Kumar, and P. S. Raju (2007), Mantle deformation in Sikkim and adjoining Himalaya: Evidence for a complex flow pattern, *Phys. Earth Planet. Inter.*, *164*, 232–241, doi: 10.1016/j.pepi.2007.07.003.
- Sol, S., et al. (2007), Geodynamics of the southern Tibetan Plateau from seismic anisotropy and geodesy, *Geology*, *35*, 563–566.
- Tatham, D. J., G. E. Lloyd, R. W. H. Butler, and M. Casey (2008), Amphibole and lower crustal seismic properties, *Earth Planet. Sci. Lett.*, *267*, 118–128.
- Tilmann, F., et al. (2003), Seismic imaging of the downwelling Indian lithosphere beneath central Tibet, *Science*, *300*, 1424–1427.
- Vinnik, L. P., L. I. Makeyeva, A. Milev, and A. Y. Usenko (1992), Global patterns of azimuthal anisotropy and deformations in the continental mantle, *Geophys. J. Int.*, *111*, 433–447.
- Wang, C. Y., L. M. Flesch, P. G. Silver, L. J. Chang, and W. W. Chan (2008), Evidence for mechanically coupled lithosphere in central Asia and resulting implications, *Geology*, *36*, 363–366.
- Yin, A., and T. M. Harrison (2000), Geologic evolution of the Himalayan-Tibetan orogen, *Annu. Rev. Earth Planet. Sci.*, *28*, 211–280.
- Zhang, P.-Z., et al. (2004), Continuous deformation of the Tibetan Plateau from global positioning system data, *Geology*, *32*, 809–812.
- Zhang, S., and S. I. Karato (1995), Lattice preferred orientation of olivine aggregates deformed in simple shear, *Nature*, *375*, 774–777.